

Measurement of Stimulated Raman Side-Scattering Energetic Importance in Directly Driven Experiment

K. Glize,^{1,2,*} X. Zhao,^{1,2,*} Y. H. Zhang,^{3,2} C. W. Lian,⁴ S. Tan,⁵ F. Y. Wu,^{1,2}
C. Z. Xiao,⁵ R. Yan,⁶ Z. Zhang,^{3,2,7} X. H. Yuan,^{1,2,†} and J. Zhang^{1,2,3,†}

¹*Key Laboratory for Laser Plasmas (MoE) and School of Physics and Astronomy,
Shanghai Jiao Tong University, Shanghai 200240, China*

²*Collaborative Innovation Center of IFSA (CICIFSA),
Shanghai Jiao Tong University, Shanghai 200240, China*

³*Beijing National Laboratory for Condensed Matter Physics,
Institute of Physics, Chinese Academy of Sciences, Beijing 100190, China*

⁴*Department of Plasma Physics and Fusion Engineering and CAS Key Laboratory of Geospace Environment,
University of Science and Technology of China, Hefei, Anhui 230026, China*

⁵*Key Laboratory for Micro-/Nano-Optoelectronic Devices of Ministry of Education,
School of Physics and Electronics, Hunan University, Changsha, 410082, China*

⁶*Department of Modern Mechanics, University of Science and Technology of China, Hefei, Anhui 230026, China*

⁷*Songshan Lake Materials Laboratory, Dongguan, Guangdong 523808, China*

Due to its particular geometry, stimulated Raman side-scattering (SRSS) drives scattered light emission at non-conventional directions, leading to scarce and complex experimental observations. Direct-irradiation campaigns at the SG-II UP facility have measured the scattered light driven by SRSS over a wide range of angles. It indicated an emission at large polar angles over a broad azimuthal range, sensitive to the plasma profile and laser polarization, resulting in a loss of about 5% of the total laser energy. Direct comparison with back-scattering measurement has evidenced SRSS as the dominant Raman scattering process. The predominance of SRSS was confirmed by 2D particle-in-cell simulations, and its angular spread has been corroborated by ray-tracing simulations. The main implication is that a complete characterization of the SRS instability and an accurate measurement of the energy losses require the collection of the scattered light in a broad range of directions. Otherwise, spatially limited measurement could lead to an underestimation of the energetic importance of stimulated Raman scattering.

Despite the recent breakthrough in reaching thermonuclear fusion ignition in the laboratory [1], laser-plasma instabilities (LPIs) [2] remain an obstacles limiting the achievable gain in inertial confinement fusion (ICF) experiments [3]. Stimulated Raman scattering (SRS) is a three-wave coupling resonantly driving an electron plasma wave (EPW) [4]. This process leads to the scattering of a part of the incident laser reducing the energy coupling, and generation of a hot electron population that can preheat the fuel core. This instability is of primary concern in most of the ICF schemes, such as Indirect-Drive [5–7], Direct-Drive [8–10], Shock Ignition [11–16] and the more recent Double-Cone Ignition [17]. Stimulated Raman side-scattering (SRSS) is a particular SRS geometry in which the scattered light is emitted perpendicular to the density gradient, enabling an absolute growth (exponential growth in time at a localised spatial position) at density lower than $n_c/4$, where n_c is the critical density. Despite extensive theoretical investigations in the late 70s [18–20], most of the interest has been focused on stimulated Raman back-scattering (SRBS) [6], due to the experimental complexity to measure SRSS and the largest SRS growth rate for the backward geometry. Recently, there has been a renewed interest due to observations of SRSS on several planar direct-drive experiments [8–10, 12, 16, 21, 22], either from single beam interaction, or by multiple beams [23]. Multi-beam processes

happen when the laser beams are sharing a common symmetry axis enabling to drive a shared daughter wave, being either an EPW [24] or a scattered wave [21, 22]. These experimental observations have led to the development of a more complete analytical description of the SRSS, accounting for the convective nature (finite spatial amplification while propagating through the resonant region) of the instability near the turning point, in order to explain the SRSS growth in region below the absolute threshold [25]. It highlighted that ICF experiments are prone to being SRSS unstable as the instability can extend to lower densities in the convective regime due to the large dimensions of the interaction, namely long density scale-length, large laser focal spot and high temperature. Therefore a complete understanding of this detrimental process is imperative as leading to additional laser energy coupling loss and hot electron generation. However, experimental observations have been restricted to a limited number of directions since ICF laser facilities are usually not designed to measure SRS in directions other than back-scattering. Thus, comprehensive measurements of this mechanism and related losses are still not available. In order to improve the overall characterisation of SRSS, crucial new diagnostics are currently being implemented in order to provide further observations at additional angles of observations [26].

In this Letter, we present, up to our knowledge, the

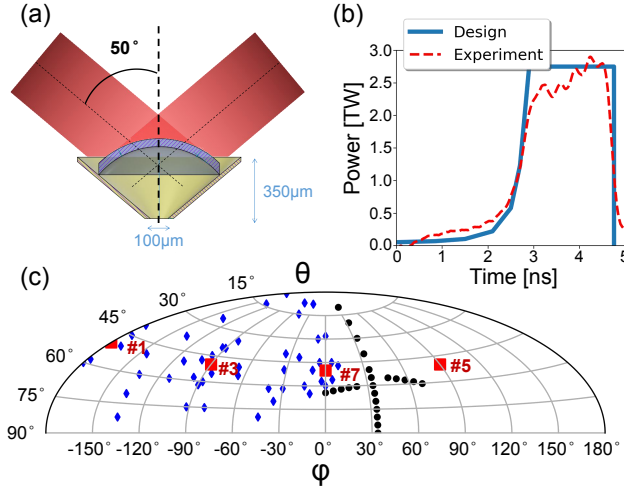


Figure 1. (a) Schematic of the irradiation geometry on the spherical target. (b) Pulse shape of the overlapped power delivered on target, both design (blue) and experimental (dashed red). (c) Spherical coordinate map depicting the positions of the laser beams (red squares), the ARSDS fibers (black dots) and the additional 50 fibers (blue diamonds).

first highly-resolved 2D angular measurement of SRS evidencing the importance of side-scattering in Direct-Drive ICF experiments. During these experimental campaigns, a new diagnostic has been designed and implemented to provide an angularly resolved measurement of the SRS emission spectrum: Angular-Resolved Scattered-light Diagnostic Station (ARSDS) [27]. It enabled to observe broadband SRS light emitted over a wide spatial area. Direct comparison with the back-scattered light collected in the aperture of one of the driver beam evidenced SRSS as the dominant SRS process. 2D PIC simulations confirmed that in this regime, the interaction was below the threshold for the typical SRBS to grow and only SRSS was responsible for the SRS emission. Due to its broad spatial emission, SRSS was identified to be responsible for the scattering of up to $5 \pm 2\%$ of the total laser energy and requires to be measured over the whole interaction volume.

The experiment was performed at the SG-II UP laser facility [28] using the setup displayed on Fig. 1(a). Two kinds of target, most commonly considered in Direct-Drive related experiments, have been used: (i) $50\mu\text{m}$ -thick CH planar target; (ii) $45\mu\text{m}$ -thick CH spherical cap target, with an inner radius of $450\mu\text{m}$. Due to the limited amount of beams, the CH cap was contained within a $20\mu\text{m}$ -thick, open-ended Au cone in order to maintain a spherical compression [17]. A cone of four beams, #1, #3, #5 and #7, were incident on the CH target at a polar angle of $\theta = 50^\circ$, uniformly distributed in the azimuthal direction. For clarity, we define here that beam #7 azimuthal position is the origin $\varphi = 0^\circ$ of the azimuth axis and that the north pole is the ori-

gin $\theta = 0^\circ$ of the polar axis. The beams are primarily p-polarised plus an angle of 7° for beams #3, #5 and 23° for beams #1, #7. Each beam delivers 1.5 kJ at 351 nm focused by a $f/7.1$ wedged lens on target within a $525\mu\text{m}$ ($1/e^2$), CPP smoothed focal spot, with a pulse shape presented on Fig. 1(b), reaching a peak overlapped intensity on target of $\approx 1.2 \times 10^{15}\text{ W.cm}^{-2}$ in vacuum. At peak power, plasma parameters were estimated using the hydro-radiative code MULTI2D [29], predicting a density scale-length of $L_{n_c/4} \approx 250\mu\text{m}$ (resp. $\approx 175\mu\text{m}$) at $n_c/4$ up to $L_{n_c/10} \approx 350\mu\text{m}$ (resp. $\approx 250\mu\text{m}$) in the coronal plasma for planar target (resp. spherical target), with a uniform electron temperature from $T_e \approx 2.0$ to 2.5 keV . The electron temperature near $n_c/4$ was confirmed to be $\leq 2.2\text{ keV}$ from the red shifted-spectral feature related to Two-Plasmon Decay (TPD) instability [30], as shown by the inset in Fig. 2(a). A Full-Aperture Back-scattering Station (FABS) was installed on #7 in order to collect the light scattered in the backward direction $[\theta, \varphi] = [50^\circ, 0^\circ]$. ARSDS was used to measure the temporally integrated SRS spectra resolved in angle for both azimuthal and polar axes. This diagnostic consists of three arrays of fibers placed 50 cm away from the target, coupled to an imaging spectrometer, collecting the scattered light at the coordinates depicted by the black dots in Fig. 1(c).

A typical result is presented on Fig. 2, displaying the scattered light spectrum angularly resolved in the (a, c) polar and (b, d) azimuthal directions for spherical and planar targets respectively. In both cases, the overall signal is dominated by light with a spectrum ranging from 530 nm up to 640 nm emitted within a wide area ranging from 30° up to 90° polar angles, over the whole azimuth, corresponding to a density range of $\approx [0.1 - 0.2]n_c$. The plain red curves on Fig. 2(e), (f), (g) and (h) present respectively the signal from Fig. 2(a), (b), (c) and (d) integrated over the spectrum, calibrated in energy and normalised to the solid angle. It shows that most of the scattered light is emitted at large polar angles, peaked around $\theta = 70^\circ$ for the spherical target, and $\theta = 75^\circ$ in the planar case. Such signal corresponds to an SRS emission at shorter wavelength and larger angle than previously reported, where usually the detection of SRS light is limited to angles $\leq 50^\circ$. Furthermore, Fig. 2(f) and (h) show that the amount of scattered energy is sensitive to the azimuthal position. For the spherical case, the maximum emission is not contained in the azimuthal plane of the laser beam but is offset by an angle $\Delta\varphi \approx 10^\circ$.

Considering that the broadband signal is emitted at polar angles larger than the incident driver beams, over a large azimuthal section, it evidences that side-scattering is responsible for such emission. The SRSS scattered light is emitted orthogonal to the density gradient and experiences refraction on its way out of the plasma [20, 25]. This results in a correlation between the scattered light wavelength and the polar exit angle, as observed on Fig. 2(a) and (c). Moreover, SRSS scattered light is also emit-

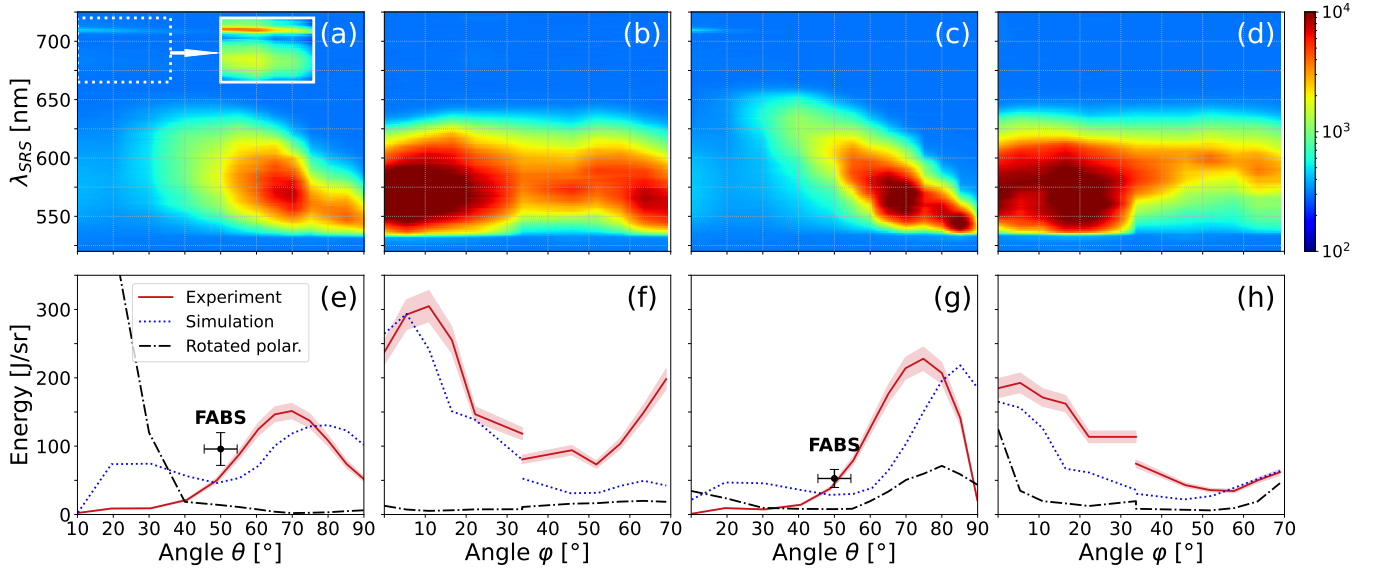


Figure 2. Typical ARSDS spectrum of the SRS emission, for spherical and planar targets respectively, against (a, c) the polar angle collected at an azimuthal angle of 33.7° ; (b, d) the azimuthal angle collected at polar angles displayed in Fig. 1(c). The inset in (a) presents the contrast enhanced TPD features. (e), (f), (g) and (h) Red plain line is the scattered energy against the exit angle, integrated over the respective spectrum and normalized to the collection solid angle. Back-scattered energy measured by FABS is displayed as a black dot on (e) and (g). The discontinuity in (f) and (h) is due to the different polar coordinate, as shown in Fig. 1(c). The blue dotted and black dash-dot lines present the scattered light signal in arbitrary units from the ray-tracing simulations with actual and rotated polarization.

ted perpendicular to the laser polarization plane, as reported in theoretical [2, 20, 31] and numerical [32–34] studies.

Due to the 2D plasma expansion, the inherent sensitivity of SRSS to the plasma profile and laser polarization, numerical simulations are required to confirm the observed angular spread of the scattered light. A new 3D ray-tracing code PHANTAM [35], based on the method published by Kaiser [36], has been developed to simulate the propagation of the SRSS light, also accounting for collisional absorption. The simulation box is $0.4 \times 0.4 \times 0.3$ cm with a $200 \times 200 \times 300$ mesh, containing a plasma obtained from the hydrodynamic simulations. SRSS light is generated when incident rays propagate into the electron density range $[0.12, 0.20]n_c$, at the associated wavelength, consistent with the experimental data, without gain nor threshold consideration. SRSS rays are initialized perpendicular to both the local density gradient and the local polarization of the incident ray with a 9-degree random spreading angle. Upon exiting the plasma, SRSS rays are collected at the same positions as the ARSDS detectors. As displayed by the blue dotted curves in Fig. 2(e), (f), (g) and (h), such simulations are confirming an emission at large polar angles, maximized near the beam azimuth, despite several discrepancies. For the planar target, the agreement appears qualitatively satisfactory, despite a slight difference in the peak position for the polar emission. For the spherical target, the offset in azimuth is retrieved in

the simulation, but the second peak at large azimuthal angle is missing. The polar emission also appears to be different than the experimental observation. This is likely the result of difference in plasma profiles between the ideal spherical compression from the simulation [37] and the actual experiment. Indeed, preliminary angular filter refractometry measurement [38] (not presented here) evidenced some plasma accumulation at the edges of the Au cone, leading to the flattening of the coronal plasma, explaining the similarities in SRSS emission for both spherical and planar targets. Besides, the importance of the laser polarization is highlighted by the black dash-dot curves, showing a completely different scattering profile when the polarization of each beam is rotated by 90° . These simulations show that the scattering is a complex combination of plasma profile, polarization and single-beam contribution from beam #7 and the neighbour beam #5. Further investigations, beyond the scope of this paper, are necessary to improve numerical agreement with the experiment and will be the subject of future work.

From these spectra, it appears that the scattering is driven by single beam SRSS, as multi-beam process would drive scattered light either in the bisector plane at $\varphi \approx 45^\circ$ for a shared scattered electromagnetic wave [21, 22], or constrained to density $n_e \leq 0.12n_c$ for a shared EPW due to the large angle between two neighbouring beams [24]. This was further confirmed by experimentally measuring a two-orders-of-magnitude decrease

of the signal in the polar direction when #7 is switched off, and retrieving the overall emission profile in the ray-tracing simulations from independent beam contribution. Thus, single-beam intensity with planar profile conditions is considered in the following discussion.

In ICF experiments, SRSS can experience both absolute or convective growth, depending on the interaction conditions. In our conditions, considering oblique incidence and damping, the absolute threshold [20] is overcome for $\lambda_{SRS} \geq 550$ nm, due to the low T_e . The lower density part can be interpreted considering the convective regime [25], having a gain $G \geq 10$ for the spectral range observed experimentally. The absence of signal above 640 nm in our data is likely due to the significant re-absorption at the associated high density, as previously reported [21, 25]. At low density, the finite size of the beam is limiting the convective growth of SRSS [25], which requires a large transverse amplification length. This corresponds to a cutoff around 530 nm for a 525 μm focal spot, consistent with our experimental observations.

FABS measurements typically show a similar spectrum and amount of scattered energy than ARSDS (up to ≈ 1.5 higher), for the same polar angle as shown on the Fig. 2(e) and (g), despite the difference in azimuth, consistent with Fig. 2(f) and (h). Such measurement evidences that there is no stronger emission localised in the backward direction which could be attributed to SRBS. This is expected as the laser intensity is one order of magnitude lower than the predicted SRBS threshold of $\approx 3 \times 10^{15} \text{ W.cm}^{-2}$ for our conditions [2, 6, 39]. Such conditions also prevents SRBS to grow from the high intensity speckles [40, 41], which have been inferred to reach up to $\approx 2.5 \times 10^{15} \text{ W.cm}^{-2}$. This results in a negligible reflectivity measured by FABS, $\leq 0.15 \pm 0.05\%$, as being only a fraction of the total scattered energy. In order to account for the large scattering angular spread, 50 additional fibers [42] were used along with ARSDS and FABS in order to extend the spatial measurement over $\frac{4}{3}\pi$, as depicted on Fig. 1(c). This diagnostic setup is similar to ARSDS, providing an energy measurement of SRS scattering integrated in time. Despite inherent uncertainties due to the limited number of directions probed, a reflectivity up to $5 \pm 2\%$ of the total laser energy was estimated, without considering the absorption. This evidences that SRSS is energetically significant and necessitates to be measured over the whole interaction volume. This implies that SRSS can lead to additional losses not usually accounted for and could be one candidate to explain some “missing” energy reported in recent experiments [7, 43]. Indeed, it appears that SRSS losses can be easily overlooked as only scattering a low amount of energy locally, which would normally not be detected or considered.

To confirm the predominance of SRSS over SRBS, 2D plane-wave PIC simulations have been performed using

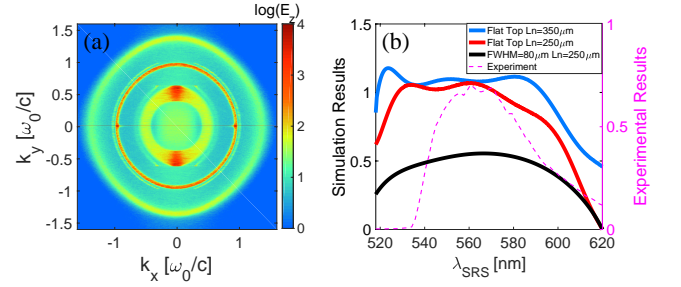


Figure 3. (a) 2D spectrum of the scattered light electric field E_z averaged over 2 ps for $L_n = 350 \mu\text{m}$ using a plane wave, (b) and associated wavelength from PIC simulations in the blue curve. Red and black lines present the scattered light wavelength for $L_n = 250 \mu\text{m}$ with a plane wave and a Gaussian wave receptively. The purple dashed lines present the signal from Fig. 2(c) integrated over the angles.

the code EPOCH [44]. An s-polarized plane wave is normally incident into a linear-density-profile plasma slab ranging from $0.1n_c$ to $0.2n_c$, with a density scale-length of 350 μm . The full simulation box is 250 μm in length (x-axis) and 100 μm in width (y-axis), and there is a 10 μm vacuum at the left boundary. The longitudinal boundary conditions are open boundary for fields and thermal boundary for particles, and the transverse boundary condition is periodic. Interaction parameters are as follow: the laser intensity $I_0 = 4.5 \times 10^{14} \text{ W.cm}^{-2}$, the electron temperature $T_e = 2 \text{ keV}$, and fixed ions. Figure 3(a) shows a time-averaged 2D spectrum of the electromagnetic wave E_z over 2 ps. The brightest signals are the near 90° scattered light perpendicular to the density gradient. As expected, there is no measurable SRBS due to its negligible convective gain. The blue curve on Fig. 3(b) is a conversion into wavelength of the scattered light spectrum from Fig. 3(a). It confirms SRSS growth over the whole range of density simulated, consistent with the experiment displayed by the purple dashed line (i.e. Fig. 2(c) integrated over the angles), despite an extension to lower wavelength for the simulation. Additional simulations with $L_n = 250 \mu\text{m}$ consistent with the spherical case, and with a finite Gaussian beam of 80 μm FWHM, have also been performed. These show identical conclusions and similar spectrum as depicted by the red and black curves respectively. The discrepancy with the experimental observation can be due to a different sensitivity of the SRSS process inherent to PIC noise.

In conclusion, the importance of stimulated Raman side-scattering in a regime usually considered SRS stable, as below the back-scattering threshold, has been experimentally observed and confirmed by 2D PIC simulations. Due to the sensitivity to both plasma profile and laser polarization, SRSS scattered light is emitted over a wide volume, as observed experimentally and confirmed by ray-tracing simulations. Such broad angular scattering results in a small amount of energy being scattered lo-

cally, while being energetically significant when measured over the whole interaction volume. Thus, our results are highlighting the necessity to use diagnostic methods with large spatial detection and high sensitivity to accurately measure SRS activity. Indeed, relying on limited directions to diagnose SRS, such as back-scattering, could lead to a strong underestimation of the actual energy losses, by a factor of 35 in our conditions. However, these results have been obtained at reduced plasma conditions compared to ignition-scale Direct-Drive experiments. Thus, further investigations are required to assess the impact of SRSS under these conditions, such as: (i) the competition between Raman side- and back-scattering when SRBS threshold is overcome; (ii) the effect of laser smoothing techniques such as smoothing by spectral dispersion (SSD) [45] which could reportedly mitigate SRSS [46]; (iii) SRSS behavior at higher intensities relevant to the Shock Ignition approach [47].

We thank the SG-II UP operating group and target fabrication team for their assistance. This work was supported by the Strategic Priority Research Program of Chinese Academy of Sciences (grants No. XDA25010100, No. XDA25030200, No. XDA25050700 & No. XDA25050400).

* These two authors contributed equally

† Authors to whom correspondence should be addressed
xiaohui.yuan@sjtu.edu.cn and jzhang1@sjtu.edu.cn

- [1] H. Abu-Shawareb and al (Indirect Drive ICF Collaboration), *Phys. Rev. Lett.* **129**, 075001 (2022).
- [2] W. L. Kruer, *Journal of Plasma Physics* **45**, 135 (1991).
- [3] J. Nuckolls, L. Wood, A. Thiessen, and G. Zimmeran, *Nature* **239**, 139 (1972).
- [4] G. G. Comisar, *Phys. Rev.* **141**, 200 (1966).
- [5] R. K. Kirkwood, J. D. Moody, J. Kline, E. Dewald, S. Glenzer, L. Divol, P. Michel, D. Hinkel, R. Berger, E. Williams, J. Milovich, L. Yin, H. Rose, B. MacGowan, O. Landen, M. Rosen, and J. Lindl, *Plasma Physics and Controlled Fusion* **55**, 103001 (2013).
- [6] D. S. Montgomery, *Physics of Plasmas* **23**, 055601 (2016), <https://doi.org/10.1063/1.4946016>.
- [7] G. N. Hall, O. S. Jones, D. J. Strozzi, J. D. Moody, D. Turnbull, J. Ralph, P. A. Michel, M. Hohenberger, A. S. Moore, O. L. Landen, L. Divol, D. K. Bradley, D. E. Hinkel, A. J. Mackinnon, R. P. J. Town, N. B. Meezan, L. Berzak Hopkins, and N. Izumi, *Physics of Plasmas* **24**, 052706 (2017).
- [8] M. J. Rosenberg, A. A. Solodov, J. F. Myatt, W. Seka, P. Michel, M. Hohenberger, R. W. Short, R. Epstein, S. P. Regan, E. M. Campbell, T. Chapman, C. Goyon, J. E. Ralph, M. A. Barrios, J. D. Moody, and J. W. Bates, *Phys. Rev. Lett.* **120**, 055001 (2018).
- [9] M. J. Rosenberg, A. A. Solodov, W. Seka, R. K. Follett, J. F. Myatt, A. V. Maximov, C. Ren, S. Cao, P. Michel, M. Hohenberger, J. P. Palastro, C. Goyon, T. Chapman, J. E. Ralph, J. D. Moody, R. H. H. Scott, K. Glize, and S. P. Regan, *Physics of Plasmas* **27**, 042705 (2020), <https://doi.org/10.1063/1.5139226>.
- [10] M. J. Rosenberg, A. A. Solodov, J. F. Myatt, S. Hironaka, J. Sivajeyan, R. K. Follett, T. Filkins, A. V. Maximov, C. Ren, S. Cao, P. Michel, M. S. Wei, J. P. Palastro, R. H. H. Scott, K. Glize, and S. P. Regan, *Physics of Plasmas* **submitted** (2022).
- [11] R. H. H. Scott, K. Glize, L. Antonelli, M. Khan, W. Theobald, M. Wei, R. Betti, C. Stoeckl, A. G. Seaton, T. D. Arber, D. Barlow, T. Goffrey, K. Bennett, W. Garbett, S. Atzeni, A. Casner, D. Batani, C. Li, and N. Woolsey, *Phys. Rev. Lett.* **127**, 065001 (2021).
- [12] G. Cristoforetti, L. Antonelli, D. Mancelli, S. Atzeni, F. Baffigi, F. Barbato, D. Batani, G. Boutoux, F. D'Amato, J. Dostal, R. Dudzak, E. Filippov, Y. J. Gu, L. Juha, O. Klimo, M. Krus, S. Malko, A. S. Martynenko, P. Nicolai, V. Ospina, S. Pikuz, O. Renner, J. Santos, V. T. Tikhonchuk, J. Trela, S. Viciani, L. Volpe, S. Weber, and L. A. Gizzi, *High Power Laser Science and Engineering* **7** (2019), 10.1017/hpl.2019.37.
- [13] G. Cristoforetti, S. Hüller, P. Koester, L. Antonelli, S. Atzeni, F. Baffigi, D. Batani, C. Baird, N. Booth, M. Galimberti, K. Glize, A. Héron, M. Khan, P. Loiseau, D. Mancelli, M. Notley, P. Oliveira, O. Renner, M. Smid, A. Schiavi, G. Tran, N. C. Woolsey, and L. A. Gizzi, *High Power Laser Science and Engineering* **9**, e60 (2021).
- [14] S. Baton, A. Colaitis, C. Rousseaux, G. Boutoux, S. Brygoo, L. Jacquet, M. Koenig, D. Batani, A. Casner, E. L. Bel, D. Raffestin, A. Tentori, V. Tikhonchuk, J. Trela, C. Reverdin, L. Le-Deroff, W. Theobald, G. Cristoforetti, L. Gizzi, P. Koester, L. Labate, and K. Shigemori, *High Energy Density Physics* **36**, 100796 (2020).
- [15] D. Barlow, T. Goffrey, K. Bennett, R. H. H. Scott, K. Glize, W. Theobald, K. Anderson, A. A. Solodov, M. J. Rosenberg, M. Hohenberger, N. C. Woolsey, P. Bradford, M. Khan, and T. D. Arber, *Physics of Plasmas* **29**, 082704 (2022), <https://doi.org/10.1063/5.0097080>.
- [16] A. Ruocco, K. Glize, A. Nutter, M. J. Rosenberg, A. A. Solodov, T. Arber, K. Goffrey, K. Bennet, S. Morris, S. J. Spencer, and R. H. H. Scott, *Matter and Radiation at Extremes* **in preparation** (2022).
- [17] J. Zhang, W. M. Wang, X. H. Yang, D. Wu, Y. Y. Ma, J. L. Jiao, Z. Zhang, F. Y. Wu, X. H. Yuan, Y. T. Li, and J. Q. Zhu, *Philosophical Transactions of the Royal Society A: Mathematical, Physical and Engineering Sciences* **378**, 20200015 (2020), <https://doi/pdf/10.1098/rsta.2020.0015>.
- [18] C. S. Liu, M. N. Rosenbluth, and R. B. White, *The Physics of Fluids* **17**, 1211 (1974), <https://aip.scitation.org/doi/pdf/10.1063/1.1694867>.
- [19] M. A. Mostrom and A. N. Kaufman, *Phys. Rev. Lett.* **42**, 644 (1979).
- [20] B. B. Afeyan and E. A. Williams, *The Physics of Fluids* **28**, 3397 (1985), <https://aip.scitation.org/doi/pdf/10.1063/1.865340>.
- [21] S. Depierreux, C. Neuville, C. Baccou, V. Tassin, M. Casanova, P.-E. Masson-Laborde, N. Borisenko, A. Orekhov, A. Colaitis, A. Debayle, G. Duchateau, A. Heron, S. Huller, P. Loiseau, P. Nicolaï, D. Pesme, C. Riconda, G. Tran, R. Bahr, J. Katz, C. Stoeckl, W. Seka, V. Tikhonchuk, and C. Labaune, *Phys. Rev. Lett.* **117**, 235002 (2016).
- [22] S. Depierreux, C. Neuville, V. Tassin, M.-C. Monteil, P.-E. Masson-Laborde, C. Baccou, P. Fremerye,

- F. Philippe, P. Seytor, D. Teychenné, J. Katz, R. Bahr, M. Casanova, N. Borisenko, L. Borisenko, A. Orekhov, A. Colaitis, A. Debayle, G. Duchateau, A. Heron, S. Huller, P. Loiseau, P. Nicolai, C. Riconda, G. Tran, C. Stoeckl, W. Seka, V. Tikhonchuk, D. Pesme, and C. Labaune, *Plasma Physics and Controlled Fusion* **62**, 014024 (2019).
- [23] R. W. Short, *Physics of Plasmas* **27**, 042703 (2020), <https://doi.org/10.1063/1.5131158>.
- [24] P. Michel, L. Divol, E. L. Dewald, J. L. Milovich, M. Hohenberger, O. S. Jones, L. B. Hopkins, R. L. Berger, W. L. Kruer, and J. D. Moody, *Phys. Rev. Lett.* **115**, 055003 (2015).
- [25] P. Michel, M. J. Rosenberg, W. Seka, A. A. Solodov, R. W. Short, T. Chapman, C. Goyon, N. Lemos, M. Hohenberger, J. D. Moody, S. P. Regan, and J. F. Myatt, *Phys. Rev. E* **99**, 033203 (2019).
- [26] M. J. Rosenberg, J. E. Hernandez, N. Butler, T. Filkins, R. E. Bahr, R. K. Jungquist, M. Bedzyk, G. Swadling, J. S. Ross, P. Michel, N. Lemos, J. Eichmiller, R. Sommers, P. Nyholm, R. Boni, J. A. Marozas, R. S. Craxton, P. W. McKenty, A. Sharma, P. B. Radha, D. H. Froula, P. Datte, M. Gorman, J. D. Moody, J. M. Heinmiller, J. Fornes, P. Hillyard, and S. P. Regan, *Review of Scientific Instruments* **92**, 033511 (2021), <https://doi.org/10.1063/5.0040558>.
- [27] X. Zhao, X. H. Yuan, J. Zheng, Y. F. Dong, K. Glize, Y. H. Zhang, Z. Zhang, and J. Zhang, *Review of Scientific Instruments* **93**, 053505 (2022), <https://doi.org/10.1063/5.0090841>.
- [28] G. Xu, T. Wang, Z. Li, Y. Dai, Z. Lin, Y. Gu, and J. Zhu, *The Review of Laser Engineering* **36**, 1172 (2008).
- [29] R. Ramis, J. M. ter Vehn, and J. Ramírez, *Computer Physics Communications* **180**, 977 (2009).
- [30] W. Seka, B. B. Afeyan, R. Boni, L. M. Goldman, R. W. Short, K. Tanaka, and T. W. Johnston, *The Physics of Fluids* **28**, 2570 (1985), <https://aip.scitation.org/doi/pdf/10.1063/1.865265>.
- [31] C. R. Menyuk, N. M. El-Siragy, and W. M. Manheimer, *The Physics of Fluids* **28**, 3409 (1985), <https://aip.scitation.org/doi/pdf/10.1063/1.865341>.
- [32] C. Z. Xiao, Z. J. Liu, C. Y. Zheng, and X. T. He, *Physics of Plasmas* **23**, 022704 (2016), <https://doi.org/10.1063/1.4941969>.
- [33] C. Z. Xiao, H. B. Zhuo, Y. Yin, Z. J. Liu, C. Y. Zheng, Y. Zhao, and X. T. He, *Plasma Physics and Controlled Fusion* **60**, 025020 (2018).
- [34] Y.-J. Gu, O. Klimo, V. Tikhonchuk, and S. Weber, *Nuclear Fusion* **61**, 066014 (2021).
- [35] Y. Ji, C. W. Lian, and R. Yan, **in preparation** (2022).
- [36] T. B. Kaiser, *Phys. Rev. E* **61**, 895 (2000).
- [37] M. Q. Yang, F. Y. Wu, Z. B. Chen, Y. X. Zhang, Y. Chen, J. C. Zhang, Z. Z. Chen, Z. F. Fang, R. Ramis, and J. Zhang, *Acta Physica Sinica* **71**, 225202 (2022).
- [38] D. Haberberger, S. Ivancic, S. X. Hu, R. Boni, M. Barczys, R. S. Craxton, and D. H. Froula, *Physics of Plasmas* **21**, 056304 (2014), <https://doi.org/10.1063/1.4873899>.
- [39] K. Estabrook and W. L. Kruer, *The Physics of Fluids* **26**, 1892 (1983), <https://aip.scitation.org/doi/pdf/10.1063/1.864336>.
- [40] C. Rousseaux, K. Glize, S. D. Baton, L. Lancia, D. Bénisti, and L. Gremillet, *Phys. Rev. Lett.* **117**, 015002 (2016).
- [41] K. Glize, C. Rousseaux, D. Bénisti, V. Dervieux, L. Gremillet, S. D. Baton, and L. Lancia, *Physics of Plasmas* **24**, 032708 (2017), <https://doi.org/10.1063/1.4978879>.
- [42] Y. H. Zhang, *Review of Scientific Instruments in preparation* (2022).
- [43] D. Turnbull, J. Katz, D. E. Hinkel, P. Michel, T. Chapman, L. Divol, E. Kur, S. MacLaren, A. L. Milder, M. Rosen, A. Shvydky, G. B. Zimmerman, and D. H. Froula, *Phys. Rev. Lett.* **129**, 025001 (2022).
- [44] T. D. Arber, K. Bennett, C. S. Brady, A. Lawrence-Douglas, M. G. Ramsay, N. J. Sircombe, P. Gillies, R. G. Evans, H. Schmitz, A. R. Bell, and C. P. Ridgers, *Plasma Physics and Controlled Fusion* **57**, 113001 (2015).
- [45] S. Skupsky, R. W. Short, T. Kessler, R. S. Craxton, S. Letzring, and J. M. Soures, *Journal of Applied Physics* **66**, 3456 (1989), <https://doi.org/10.1063/1.344101>.
- [46] N. Kang, H. Liu, S. Zhou, Y. Zhao, and A. Lei, *J. Opt. Soc. Am. B* **38**, 3567 (2021).
- [47] R. Betti, C. D. Zhou, K. S. Anderson, L. J. Perkins, W. Theobald, and A. A. Solodov, *Phys. Rev. Lett.* **98**, 155001 (2007).